Monthly Notices
of the
ROYAL ASTRONOMICAL SOCIETY

MNRAS **440,** 3645–3657 (2014) doi:10.1093/mnras/stu543

The thermal Sunyaev–Zel'dovich effect power spectrum in light of *Planck*

I. G. McCarthy,[1⋆] A. M. C. Le Brun,[1] J. Schaye[2] and G. P. Holder[3]

[1]*Astrophysics Research Institute, Liverpool John Moores University, 146 Brownlow Hill, Liverpool L3 5RF, UK*
[2]*Leiden Observatory, Leiden University, PO Box 9513, NL-2300 RA Leiden, the Netherlands*
[3]*Department of Physics, McGill University, 3600 Rue University, Montreal, Quebec H3A 2T8, Canada*

Accepted 2014 March 16. Received 2014 March 12; in original form 2013 December 18

ABSTRACT

The amplitude of the thermal Sunyaev–Zel'dovich effect (tSZ) power spectrum is extremely sensitive to the abundance of the most massive dark matter haloes (galaxy clusters) and therefore to fundamental cosmological parameters that control their growth, such as σ_8 and $\Omega_{\rm m}$. Here we explore the sensitivity of the tSZ power spectrum to important non-gravitational ('subgrid') physics by employing the cosmo-OWLS suite of large-volume cosmological hydrodynamical simulations, run in both the *Planck* and 7-year *Wilkinson Microwave Anisotropy Probe* (*WMAP*7) best-fitting cosmologies. On intermediate and small angular scales ($\ell \gtrsim 1000$, or $\theta \lesssim 10$ arcmin), accessible with the South Pole Telescope (SPT) and the Atacama Cosmology Telescope (ACT), the predicted tSZ power spectrum is highly model dependent, with gas ejection due to active galactic nuclei (AGN) feedback having a particularly large effect. However, at large scales, observable with the *Planck* telescope, the effects of subgrid physics are minor. Comparing the simulated tSZ power spectra with observations, we find a significant amplitude offset on all measured angular scales (including large scales), if the *Planck* best-fitting cosmology is assumed by the simulations. This is shown to be a generic result for all current models of the tSZ power spectrum. By contrast, if the *WMAP*7 cosmology is adopted, there is full consistency with the *Planck* tSZ power spectrum measurements on large scales and agreement at the 2σ level with the SPT and ACT measurements at intermediate scales for our fiducial AGN model, which Le Brun et al. have shown reproduces the 'resolved' properties of the Local Group and cluster population remarkably well. These findings strongly suggest that there are significantly fewer massive galaxy clusters than expected for the *Planck* best-fitting cosmology, which is consistent with recent measurements of the tSZ number counts. Our findings therefore pose a significant challenge to the cosmological parameter values preferred (and/or the model adopted) by the *Planck* primary cosmic microwave background analyses.

Key words: galaxies: clusters: general – galaxies: clusters: intracluster medium – cosmic background radiation – cosmological parameters – cosmology: theory.

1 INTRODUCTION

The hot gas in galaxy groups and clusters, called the intracluster medium (ICM), acts as a secondary source of anisotropies in the cosmic microwave background (CMB). CMB photons passing through a cluster are on average likely to inverse Compton scatter off hot electrons in the ICM, which gives the photons a small energy kick. This produces a slight intensity/temperature decrement at radio wavelengths and a slight increment at millimetre wavelengths, known as the thermal Sunyaev–Zel'dovich effect (hereafter tSZ; Sunyaev & Zeldovich 1972, see Birkinshaw 1999 for a review). If the cluster is moving with respect to the CMB rest frame, an additional distortion of the CMB due to the Doppler effect will also be produced, known as the kinetic Sunyaev–Zel'dovich effect (kSZ). The kSZ is significantly weaker than the tSZ, except near the tSZ null at ≈218 GHz (i.e. the frequency at which the number of photons scattered up from lower energies cancels the number of photons being scattered up to higher energies). For the present study, we concern ourselves with the tSZ only, noting that the kSZ signal has been detected for the first time only very recently (e.g. Hand et al. 2012; Sayers et al. 2013).

The tSZ signal on the sky is highly sensitive to the fundamental cosmological parameters that control the growth of galaxy clusters

⋆ E-mail: i.g.mccarthy@ljmu.ac.uk

(e.g. Carlstrom, Holder & Reese 2002; Komatsu & Seljak 2002), offering an important and independent measurement of parameters such as σ_8 and Ω_m (which can be constrained through the tSZ power spectrum amplitude and tSZ cluster number counts), as well as H_0 (by exploiting the differing dependencies of the tSZ and X-ray signals of the ICM to measure a physical size of clusters independent of their redshift) and a tool to test models of the evolution of dark energy (e.g. by measuring the redshift evolution of the number counts). It is therefore unsurprising that there are large numbers of tSZ surveys in the works [e.g. Atacama Cosmology Telescope (ACT), South Pole Telescope (SPT), *Planck*, Atacama Pathfinder Experiment-Sunyaev–Zel'dovich (APEX-SZ), Multiplexed SQUID TES Array at Ninety GHz (MUSTANG), Combined Array for Research in Millimeter-wave Astronomy (CARMA), Atacama Large Millimeter/submillimeter Array (ALMA), Arcminute Microkelvin Imager (AMI), Array for Microwave Background Anisotropy (AMiBA)].

Its use as a cosmological probe is, however, complicated by the fact that the tSZ signal is sensitive to the astrophysics governing the thermal state of the ICM, since the magnitude of the tSZ depends directly on the (line of sight integral of) pressure of the hot gas. The pressure, in turn, is set by the depth of the dark matter potential well and the entropy of the hot gas, which can be significantly altered by non-gravitational processes such as radiative cooling and feedback from processes related to galaxy formation (e.g. Voit 2005; Nagai, Kravtsov & Vikhlinin 2007; McCarthy et al. 2011). Indeed, recent studies have shown that the tSZ power spectrum is sensitive to ICM modelling details on scales of a few arcminutes (e.g. Holder, McCarthy & Babul 2007; Battaglia et al. 2010; Shaw et al. 2010; Trac, Bode & Ostriker 2011) where, until recently, tSZ power spectrum constraints have been limited to.

However, it is noteworthy that important progress has been made in recent years on modelling the effects of cooling and feedback on the ICM, so much so that reasonably realistic populations of clusters, which match a wide variety of observed properties, are now being produced in cosmological simulations (e.g. Bower, McCarthy & Benson 2008; Puchwein, Sijacki & Springel 2008; Short & Thomas 2009; McCarthy et al. 2010, 2011; Planelles et al. 2014; Le Brun et al. 2014). Furthermore, measurements of the tSZ power spectrum are now being made on larger angular scales (of a few degrees) with the *Planck* telescope (Planck Collaboration XXI 2013), which are significantly less sensitive to uncertain baryonic physics (e.g. Komatsu & Kitayama 1999). This should give a renewed emphasis on the tSZ as a cosmological probe.

In the present study, we take state-of-the-art cosmological hydrodynamical simulations and construct large simulated tSZ skies and make comparisons with the latest 'unresolved' (power spectrum) tSZ measurements from the *Planck* telescope, as well as from the SPT, and the ACT. From this comparison we arrive at the robust conclusion that there is a significant tension between existing tSZ power spectrum measurements and the cosmological parameter values preferred (and/or the model adopted) by the *Planck* primary CMB analyses (Planck Collaboration XVI 2013).

The present study is organized as follows. In Section 2 we briefly describe the cosmo-OWLS simulation suite used here and our map-making procedure. Le Brun et al. (2014) have compared these simulations with the observed properties of local groups and clusters and concluded that the fiducial active galactic nuclei (AGN) feedback model performs remarkably well, reproducing the observed trends over a wide range of halo masses and radii. In Section 3 we compare the predicted pressure distributions of the simulated groups and clusters with observations of local systems. In Section 4 we dissect the theoretical tSZ power spectra into its contributions from hot gas in haloes in bins of mass, redshift, and radius. In Section 5 we compare the predicted tSZ power spectra with observations. In Section 6 we compare our predicted tSZ power spectra with those of other models. Finally, in Section 7 we summarize and discuss our findings.

2 SIMULATIONS

We employ the cosmo-OWLS suite of cosmological hydrodynamical simulations described in detail in Le Brun et al. (2014, hereafter L14; see also van Daalen et al. 2013). cosmo-OWLS is an extension of the OWLS project (Schaye et al. 2010) designed with cluster cosmology and large-scale structure surveys in mind. The cosmo-OWLS suite consists of large-volume $(400\,h^{-1}\,\mathrm{Mpc})^3$ periodic box hydrodynamical simulations with 1024^3 baryon and dark matter particles (each) and with updated initial conditions based either on the maximum likelihood cosmological parameters derived from the 7-year *Wilkinson Microwave Anisotropy Probe* (*WMAP*) data (hereafter *WMAP*7; Komatsu et al. 2011) $\{\Omega_m, \Omega_b, \Omega_\Lambda, \sigma_8, n_s, h\} = \{0.272, 0.0455, 0.728, 0.81, 0.967, 0.704\}$ or the *Planck* data (Planck Collaboration XVI 2013) $= \{0.3175, 0.0490, 0.6825, 0.834, 0.9624, 0.6711\}$. This yields dark matter and (initial) baryon particle masses of $\approx 4.44 \times 10^9\,h^{-1}\,\mathrm{M}_\odot$ ($\approx 3.75 \times 10^9\,h^{-1}\,\mathrm{M}_\odot$) and $\approx 8.12 \times 10^8\,h^{-1}\,\mathrm{M}_\odot$ ($\approx 7.54 \times 10^8\,h^{-1}\,\mathrm{M}_\odot$) for the *Planck* (*WMAP*7) cosmology. The extension to large volumes is quite important for the present study, since the tSZ power spectrum is dominated by massive dark matter haloes with $M \sim 10^{14}\,\mathrm{M}_\odot$, which have very low space densities of $\sim 10^{-5}\,\mathrm{Mpc}^{-3}$ (e.g. Jenkins et al. 2001).

As in OWLS, the comoving gravitational softening lengths for the baryon and dark matter particles are set to 1/25 of the initial mean interparticle spacing (e.g. Mo, van den Bosch & White 2010) but are limited to a maximum physical scale of $4\,h^{-1}$ kpc (Plummer equivalent). The switch from a fixed comoving to a fixed proper softening happens at $z = 2.91$. (Note that current measurements of the tSZ power spectrum probe physical scales that are two to three orders of magnitude larger than the gravitational softening of our simulations.) We use $N_{ngb} = 48$ neighbours for the smoothed particle hydrodynamics (SPH) interpolation and the minimum SPH smoothing length is limited to 0.01 of the gravitational softening.

The simulations were run using a version of the Lagrangian TreePM-SPH code GADGET3 (last described in Springel 2005), which was significantly modified to include new 'subgrid' physics as part of the OWLS project. Starting from identical initial conditions (for a given cosmology), key parameters controlling the nature and strength of feedback are systematically varied. As in L14, we use five different physical models: NOCOOL, REF, AGN 8.0, AGN 8.5, and AGN 8.7. The NOCOOL model is a standard non-radiative ('adiabatic') model. REF is the OWLS reference model, which includes subgrid prescriptions for star formation (Schaye & Dalla Vecchia 2008), metal-dependent radiative cooling (Wiersma, Schaye & Smith 2009a), stellar evolution, mass loss, and chemical enrichment (Wiersma et al. 2009b), and a kinetic supernova feedback prescription (Dalla Vecchia & Schaye 2008).

The three AGN models (AGN 8.0, AGN 8.5, and AGN 8.7) include the same subgrid prescriptions as the REF model, but also include a prescription for black hole (BH) growth and feedback from AGN (Booth & Schaye 2009, a modified version of the model developed originally by Springel, Di Matteo & Hernquist 2005). The BHs

Table 1. cosmo-OWLS runs presented here and their included subgrid physics. Each model has been run in both the *WMAP*7 and *Planck* cosmologies.

Simulation	UV/X-ray background	Cooling	Star formation	SN feedback	AGN feedback	$\Delta T_{\rm heat}$
NOCOOL	Yes	No	No	No	No	...
REF	Yes	Yes	Yes	Yes	No	...
AGN 8.0	Yes	Yes	Yes	Yes	Yes	$10^{8.0}$ K
AGN 8.5	Yes	Yes	Yes	Yes	Yes	$10^{8.5}$ K
AGN 8.7	Yes	Yes	Yes	Yes	Yes	$10^{8.7}$ K

store up enough energy[1] until they are able to raise the temperature of neighbouring gas by a predefined level, $\Delta T_{\rm heat}$. The three AGN models differ only in their choice of the heating temperature $\Delta T_{\rm heat}$, which is the most critical parameter of the AGN feedback model.[2] Note that since the same amount of gas is being heated in these models, more time is required for the BHs to accrete enough mass to be able to heat neighbouring gas to a higher temperature. Thus, increasing the heating temperature leads to more *bursty* and more violent feedback.

Table 1 provides a list of the runs used here and the subgrid physics that they include. In Appendix A we present a resolution study, concluding that our simulations are reasonably well converged.

2.1 Thermal SZ effect maps

The magnitude of the tSZ is set by the dimensionless Compton y parameter, defined as

$$y \equiv \int \sigma_{\rm T} \frac{k_{\rm B} T}{m_{\rm e} c^2} n_{\rm e} \, {\rm d}l, \tag{1}$$

where $\sigma_{\rm T}$ is the Thomson cross-section, $k_{\rm B}$ is Boltzmann's constant, T is the gas temperature, $m_{\rm e}$ is the electron rest mass, c is the speed of light, and $n_{\rm e}$ is the electron number density. Thus, y is proportional to the electron pressure integrated along the observer's line of the sight, back to the epoch of reionization.

To produce Compton y maps, we stack randomly rotated and translated snapshots at differing redshifts along the line of sight (da Silva et al. 2000) back to $z = 3$. (This is sufficiently high redshift for approximate convergence in the tSZ power spectrum; see Fig. 3.) We follow the approach of Roncarelli et al. (2006, 2007) and calculate the quantity

$$\Upsilon_i \equiv \sigma_{\rm T} \frac{k_{\rm B} T_i}{m_{\rm e} c^2} \frac{m_i}{\mu_{{\rm e},i} m_{\rm H}} \tag{2}$$

for the ith gas particle. Here T_i is the temperature of the gas particle, m_i is the gas particle mass, $\mu_{{\rm e},i}$ is the mean molecular weight per free electron of the gas particle (which depends on its metallicity), and $m_{\rm H}$ is the atomic mass of hydrogen. Note that Υ_i has dimensions of area.

The total contribution to the Compton y parameter in a given pixel by the ith particle is obtained by dividing Υ_i by the physical area of the pixel at the angular diameter distance of the particle from the observer, i.e. $y_i \equiv \Upsilon_i / L^2_{{\rm pix},i}$. We adopt an angular pixel size of 2.5 arcsec, which is better than what can be achieved with current tSZ instrumentation but is similar to the spatial resolution of X-ray telescopes like *Chandra*. We opt for this high angular resolution because we are producing X-ray maps simultaneously with the tSZ maps.

Finally, we smooth y_i on to the map using the SPH smoothing kernel, adopting as the smoothing length the 3D physical smoothing length of the particle (calculated by GADGET3) divided by the angular diameter distance of the particle, i.e. the *angular* extent of the particle's smoothing length. We have verified that the exact choice of smoothing kernel or smoothing length is inconsequential for the tSZ power spectrum over the range of angular scales considered here ($\ell < 10000$, corresponding to $\theta \gtrsim 1$ arcmin), by comparing the power spectrum produced using the fiducial SPH-smoothed maps with that produced from maps generated using a simple 'nearest grid point' method (they are virtually identical).

Previous studies found that cosmic variance can be an issue for the tSZ power spectrum calculated from maps produced from self-consistent cosmological hydrodynamical simulations, due to their finite box size and therefore limited field of view (e.g. White, Hernquist & Springel 2002; Battaglia et al. 2010). Indeed, most previous simulation studies produced maps of only a few square degrees, while current observational surveys being conducted are hundreds of square degrees. Our larger simulations allow us to produce larger maps of $5^\circ \times 5^\circ$ (7200×7200 pixels), but cosmic variance is still an issue. We therefore produce 10 maps corresponding to different viewing angles (by randomly rotating and translating the boxes) for each simulation. We note that 5° corresponds approximately to the comoving length of the simulation box ($400\,h^{-1}$ Mpc) at $z = 3$. Thus, at high redshift the 10 maps will probe many of the same structures. At lower redshifts (which dominate the tSZ power spectrum, as we show in Section 4), however, the 25 deg^2 field of view occupies only a relatively small fraction of the simulated volume, and therefore the maps are effectively independent. In Appendix B we show the map-to-map scatter around the mean and median tSZ power spectra.

As an example, we show in Fig. 1 simulated Compton y maps for the five different physical models in the *Planck* cosmology, along with one in the *WMAP*7 cosmology. All maps adopt the same viewing angle (i.e. the same randomly selected rotations and translations are applied in each case). Thus, the differences between the five *Planck* cosmology maps are due entirely to differences in the subgrid physics. Particularly noticeable is the impact of AGN feedback, which ejects gas from dark matter haloes out into the intergalactic medium. The two rightmost panels compare the same physical model (the fiducial AGN model, AGN 8.0) in the two different cosmologies. The cosmological and astrophysical dependencies of the tSZ signal are easily visible by eye in Fig. 1.

[1] As in Booth & Schaye (2009) we use 1.5 per cent of the rest mass energy of accreted gas for feedback. This efficiency choice results in a reasonable match to the normalization of the local BH scaling relations (Booth & Schaye 2009, see also L14) and is insensitive to the precise value of $\Delta T_{\rm heat}$.

[2] We note that the AGN 8.0 model was referred to as 'AGN' in previous OWLS papers and was studied in McCarthy et al. (2010, 2011) with a $100\,h^{-1}$ Mpc box, a *WMAP*3 cosmology and eight times smaller particle mass.

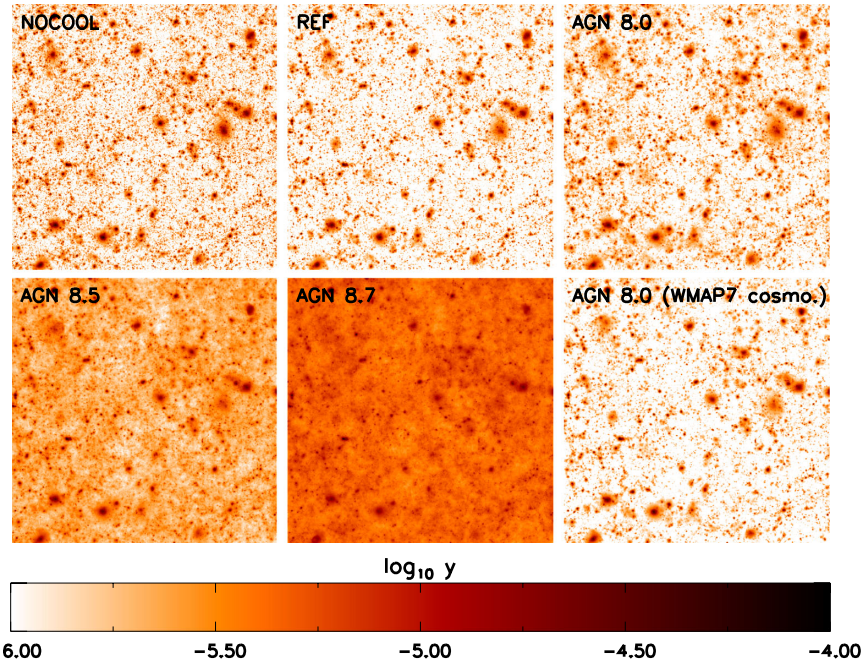

Figure 1. Example simulated Compton y maps for the five different physical models in the *Planck* cosmology, along with one in the *WMAP*7 cosmology (bottom right-hand panel). Each map is $5^\circ \times 5^\circ$ and adopts the same viewing angle (i.e. the same randomly selected rotations and translations are applied in each case). Differences between the five *Planck* cosmology maps are due entirely to differences in the subgrid physics, with gas ejection associated with AGN feedback having a particularly large effect. For a fixed physical model, the difference between the *Planck* and the *WMAP*7 cosmology is also readily visible, with more (and larger) systems present in the *Planck* cosmology run.

For each simulation we compute the tSZ angular power spectrum by averaging over the power spectra computed for each of the 10 maps.

In addition to tSZ maps, we also create halo catalogues for our light cones using a standard friends-of-friends algorithm run on the snapshot data. In Section 4 we use the halo catalogues to deconstruct the theoretical power spectra into its contributions from haloes of different mass and redshifts and from different radial ranges within the haloes.

3 PRESSURE PROFILES

Before proceeding to an analysis of the tSZ power spectrum, we first briefly (re-)examine the degree of realism of the five physical models by comparing to the observed properties of local X-ray-selected galaxy clusters. We note that L14 have already subjected these models to a full battery of observational tests at low redshift, including global X-ray, tSZ, optical, and BH scaling relations. One of the conclusions of that study is that the fiducial AGN model (AGN 8.0) reproduces virtually all of the observed local relations reasonably well (including their intrinsic scatter), while models that neglect AGN feedback (REF) suffer from significant overcooling, producing a factor of 3–5 times more mass in stars than observed. AGN models with increased heating temperatures (particularly AGN 8.7), on the other hand, eject too much gas from the progenitors of groups and clusters, yielding present-day groups and clusters with lower gas mass fractions and higher entropy than observed (it is the low-entropy gas that is preferentially heated and ejected, at high redshift). An important caveat to bear in mind, however, is that the role of observational selection is not yet well understood and this currently limits our ability to perform detailed quantitative comparisons between the models and observations (see discussion in L14).

Of direct relevance for the tSZ angular power spectrum is the electron pressure distribution of the hot gas and its dependence on halo mass and redshift, which was not examined in L14. To make a like-with-like comparison to the data, we construct synthetic X-ray observations and derive the gas density and temperature (and therefore pressure) by fitting to synthetic spatially resolved X-ray spectra (see L14 for details). We use the same synthetic observations and assume hydrostatic equilibrium to 'measure' the mass, $M_{500,\rm hse}$, and the corresponding overdensity radius $r_{500,\rm hse}$ for each of the simulated clusters.

In Fig. 2 we plot the radial electron pressure profiles of $z = 0$ groups (left-hand panel) and clusters (right-hand panel) for the various simulations and compare to X-ray observations of local, bright X-ray systems. For the observations, we compare to the *Chandra* group sample of Sun et al. (2011), while for the clusters we compare to the *XMM–Newton*/Representative *XMM–Newton* Cluster Structure Survey (REXCESS) sample (Böhringer et al. 2007). Note that this is the same data from which Arnaud et al. (2010) derived the 'universal pressure profile', which adopts a generalized Navarro–Frenk–White (NFW) form (see Nagai et al. 2007). Instead of plotting the universal pressure profile, we plot the best-fitting profiles for the individual REXCESS systems (i.e. with system-to-system scatter included).

We normalize the radial coordinate by $r_{500,\rm hse}$, the radius within which the mean mass density is 500 times the critical density for closure (which is typically the radius out to which good quality X-ray data can presently probe). We normalize the electron pressure by the 'virial pressure' $P_{500,\rm hse} \equiv n_{\rm e,500} k_{\rm B} T_{500,\rm hse}$, where $k_{\rm B} T_{500,\rm hse} \equiv \mu m_{\rm p} G M_{500,\rm hse}/2 r_{500,\rm hse}$ is the virial temperature and $n_{\rm e,500}$ is the mean electron density within $r_{500,\rm hse}$

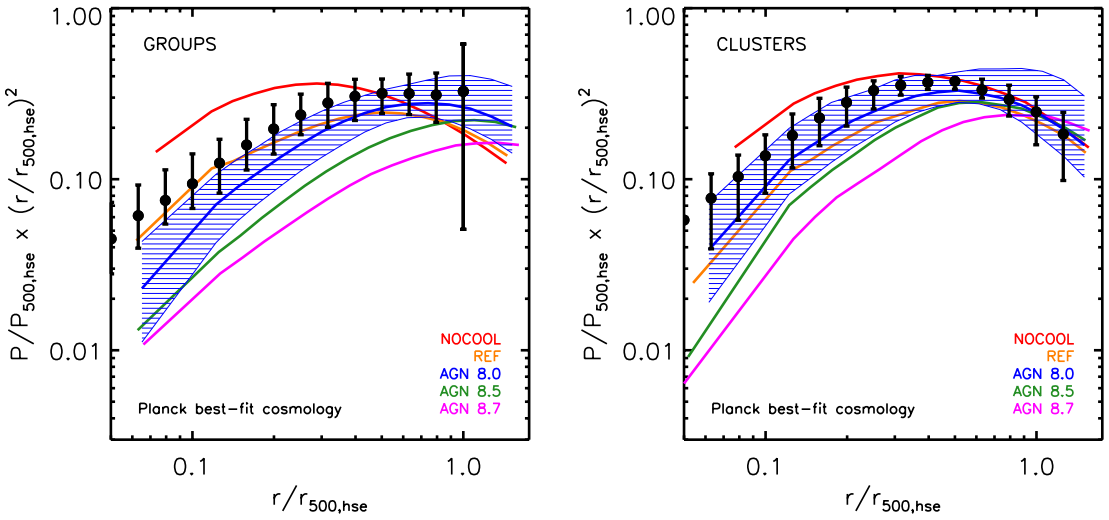

Figure 2. Radial electron pressure profiles of groups ($13 \lesssim \log[M_{500,\rm hse}h/{\rm M}_\odot] \lesssim 14.1$; left) and clusters ($13.8 \lesssim \log[M_{500,\rm hse}h/{\rm M}_\odot] \lesssim 14.8$; right) at $z \approx 0$. The filled black circles with error bars correspond to the observational data of Sun et al. (2011) (left, groups) and the REXCESS sample of Böhringer et al. (2007) and Arnaud et al. (2010) (right, clusters). The error bars enclose 68 per cent of the observed systems. The curves represent medians of the different simulations, with the shaded region enclosing 68 per cent of the simulated systems for AGN 8.0 model. The fiducial AGN model (AGN 8.0), which reproduces the local X-ray and optical scaling relations best (L14), reproduces the observed pressure profiles of groups (outside $\gtrsim 0.3r_{500}$) and clusters well.

assuming the universal baryon fraction $f_{\rm b} \equiv \Omega_{\rm b}/\Omega_{\rm m}$, i.e. $n_{\rm e,500} \equiv 500 f_{\rm b}\rho_{\rm crit}(z)/\mu_{\rm e}m_{\rm H}$. To reduce the dynamic range on the y-axis further, we scale the normalized pressure by a factor $(r/r_{500,\rm hse})^2$ for both simulations and observations. We also scale the observed pressure profiles to our adopted cosmology when comparing to the simulations (noting particularly that $P_{500,\rm hse}$ depends on the adopted $f_{\rm b}$). Lastly, as the shape and amplitude of the pressure profiles are fairly strong functions of halo mass, we have re-sampled the simulated cluster mass distribution in order to achieve approximately the same median mass as the observed samples. In particular, for the groups we select systems in the (true) mass range $5.8 \times 10^{13} < M_{500} < 1.5 \times 10^{14}\,{\rm M}_\odot$ to achieve a median mass of $M_{500,\rm hse} \approx 8.6 \times 10^{13}\,{\rm M}_\odot$, while for the cluster comparison we select systems in the mass range $2.5 \times 10^{14} < M_{500} < 10^{15}\,{\rm M}_\odot$ to achieve a median mass of $M_{500,\rm hse} \approx 3.5 \times 10^{14}\,{\rm M}_\odot$.

From Fig. 2 it is immediately apparent that the pressure distribution of the hot gas is strongly model dependent, with large differences between the models within $\sim r_{500,\rm hse}$ for groups and $\sim 0.5r_{500,\rm hse}$ for clusters. At $\sim 0.1r_{500,\rm hse}$, for example, the pressure can vary by up to an order of magnitude from model to model. The tSZ power spectrum at currently accessible angular scales is sensitive to intermediate radii (see Fig. 3), implying we should expect some sensitivity to non-gravitational physics.

Consistent with L14, we find that the fiducial AGN model (AGN 8.0) appears to perform best. The REF model, which neglects AGN feedback, performs similarly well, but at the expense of significant overcooling, i.e. too high stellar masses (not shown here, see L14). Increasing the AGN heating temperature leads to a strong suppression of the gas density at small and intermediate radii, which in turn yields electron pressures that are significantly lower than observed. However, it is important to bear in mind that at present we can only make these kind of comparisons for *local* groups and clusters, where the data quality is sufficiently high. The tSZ power spectrum, however, has a non-negligible contribution from high-redshift clusters (out to $z \sim 1.5$) and it is unclear which (if any) of the models perform reasonably well there.

4 DECONSTRUCTING THE THERMAL SZ EFFECT POWER SPECTRUM

To aid our interpretation of the comparison with observations of the tSZ power spectrum below (in Section 5), we first deconstruct the simulated tSZ power spectra into its contributions from hot gas in haloes in bins of true M_{500}, redshift, and radius. The results are plotted in Fig. 3 for the fiducial AGN model (AGN 8.0) in the *Planck* best-fitting cosmology. We discuss below how these trends depend on the choice of cosmology and subgrid physics. Note that to reduce sampling noise in the power spectra, we have re-binned to a multipole resolution of $\Delta\ell = 200$.

We consider the break down by system mass first, plotted in the top panel of Fig. 3. The coloured curves correspond to power spectra from gas within r_{200} in different M_{500} bins. At large angular scales ($\ell \lesssim 1000$), accessible by the *Planck* telescope, the power spectrum is dominated by relatively massive ($\log[M_{500}h/{\rm M}_\odot] > 14$) systems. A relatively larger contribution is made from galaxy groups with [13.5–14.0] at intermediate angular scales ($\ell \sim 3000$) observable with SPT and ACT, but clusters still dominate the signal. It is only when one approaches scales of an arcminute ($\ell \sim 10\,000$) or so that the contribution of systems with masses below $10^{14}\,h^{-1}\,{\rm M}_\odot$ becomes comparable to that from systems with masses above this limit.

The trends in the top panel of Fig. 3 are very similar for the *WMAP*7 best-fitting cosmology, but with a slightly increased importance of high-mass groups [13.5–14.0] compare to clusters [>14] on the largest scales (and low-mass groups [13.0–13.5] compared to high-mass groups [13.5–14.0] on small angular scales), due to the fact that the number density of massive haloes is significantly reduced in the *WMAP*7 cosmology compared to the *Planck* cosmology. The trends are not particularly sensitive to the nature of the implemented subgrid physics either; massive systems with $\log[M_{500}h/{\rm M}_\odot] > 14$ dominate the power spectrum at $\ell < 5000$ for all of the models we have considered. Our trends with system mass are similar to those reported previously by Battaglia et al. (2012), although there are differences in detail.

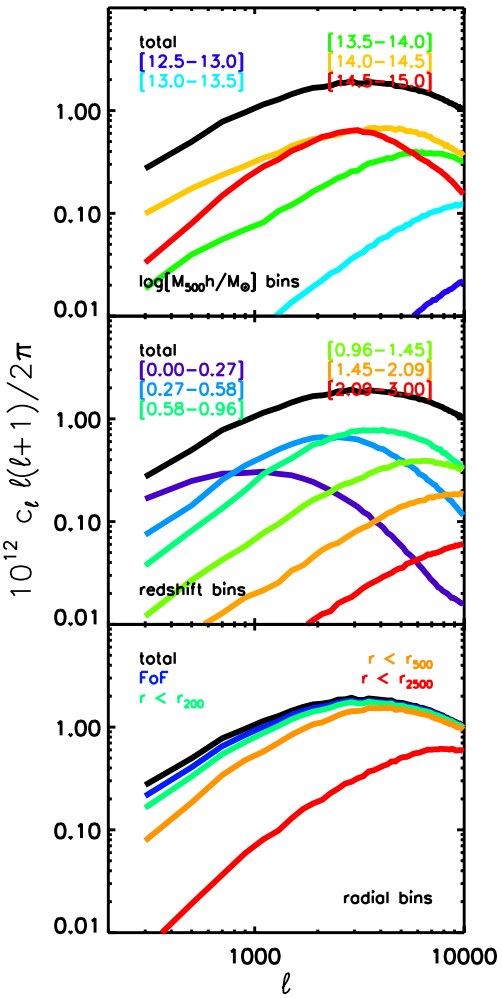

Figure 3. Deconstruction of the tSZ angular power spectrum. Shown is the contribution from hot gas in haloes in bins of $\log[M_{500}h/\mathrm{M}_\odot]$ (top), redshift (middle), and radius (bottom) for the fiducial AGN model (AGN 8.0). At large angular scales ($\ell \lesssim 1000$), accessible by *Planck*, the power spectrum is dominated by clusters ($\log M_{500}h/\mathrm{M}_\odot \gtrsim 14$), nearby ($z \lesssim 0.5$) clusters with most of the power coming from large physical scales ($r \gtrsim r_{500}$). At intermediate angular scales ($\ell \sim 3000$), observable with SPT and ACT, the signal is still dominated by clusters but over a much wider range of redshifts (out to $z \sim 1.5$) with most of the power coming from the radial range $r_{2500} \lesssim r \lesssim r_{500}$.

In the middle panel of Fig. 3 we consider the contribution from hot gas in different redshift bins. We have chosen the six redshift bins to have approximately the same comoving length (∼1 Gpc). At large angular scales ($\ell \lesssim 1000$), the power spectrum is produced mainly by relatively local systems with $z \lesssim 0.5$ but with a non-negligible contribution from gas out to $z \sim 1$. At intermediate angular scales ($\ell \sim 3000$), on the other hand, the signal has significant contributions from $0 \lesssim z \lesssim 1.5$ with the range $0.25 \lesssim z \lesssim 1$ providing the largest contribution. As one pushes to smaller angular scales ($\ell \sim 10\,000$) local sources no longer contribute significantly while gas out to $z \sim 2$ becomes important.

The trends in the middle panel of Fig. 3 are virtually identical in the *WMAP*7 best-fitting cosmology, depend only very mildly on the nature of the implemented subgrid physics, and are similar to those reported previously by Battaglia et al. (2012).

In the bottom panel of Fig. 3 we compute the contribution to the power spectrum from gas in different radial ranges. Note that r_{200} is typically taken to be the virial radius and that $r_{500} \approx 0.65 r_{200}$ and $r_{2500} \approx 0.45 r_{500}$ for a NFW profile with a typical cluster concentration of 5. The 'FoF' (blue) curve corresponds to the power spectrum from gas linked to the friends-of-friends group in which the simulated galaxy cluster lives. This includes gas within r_{200} as well as some beyond this radius. Note that the FoF region is not constrained to be spherical, but typically $M_{\mathrm{FoF}} \sim 2M_{200}$ (with significant scatter) for a standard linking length of 0.2 times the mean interparticle separation.

At large angular scales ($\ell \lesssim 1000$) most of the tSZ signal comes from large physical radii, with more than half of the power coming from beyond r_{500} (i.e. beyond the reach of most X-ray observations). At intermediate angular scales ($\ell \sim 3000$) gas within the radial range $r_{2500} \lesssim r \lesssim r_{500}$ is the largest contributor to the power spectrum. At angular scales of an arcminute and below ($\ell \sim 10\,000$), the 'inner' regions ($r \lesssim r_{2500}$) of groups and clusters begin to dominate.

The trends in the bottom panel of Fig. 3 are virtually identical in the *WMAP*7 best-fitting cosmology for a given subgrid model. The fiducial AGN model has a similar behaviour to that of the NOCOOL and REF models. However, increasing the AGN heating temperature boosts the contribution from gas at large radii on large angular scales ($\ell \lesssim 1000$), due to the efficient ejection of gas from within r_{500}.

Comparing the trends in Fig. 3 with the pressure profiles in Fig. 2, our expectation is that at the large angular scales observable by the *Planck* telescope ($\ell \lesssim 1000$), the power spectrum should be relatively insensitive to subgrid physics. That is because these scales probe very large physical radii around relatively massive clusters. By contrast, we should expect to find relatively large differences between the models at intermediate angular scales of $\ell \sim 3000$ (observable with SPT and ACT), since these probe intermediate radii ($r_{2500} \lesssim r \lesssim r_{500}$) and lower halo masses.

5 COMPARISON WITH OBSERVATIONS

In Fig. 4 we plot the predicted tSZ angular power spectra for the five models (thick colour curves) in both the *WMAP*7 (left-hand panel) and *Planck* primary CMB (right-hand panel) best-fitting cosmologies, along with the latest power spectrum measurements from the *Planck* telescope (Planck Collaboration XXI 2013), SPT (Reichardt et al. 2012), and ACT (Sievers et al. 2013) as the data points with error bars. Note that the observational error bars represent 1σ constraints on the power spectrum. In the case of the *Planck* measurements we sum the statistical and foreground uncertainties (e.g. as in fig. 15 of Planck Collaboration XXI 2013).

For the Planck best-fitting cosmology, a significant amplitude offset is present between all the models and the observations on all measured angular scales. Notably, the offset exists even at the largest angular scales, where the effects of baryon physics are minor, as can be deduced from the convergence of the models there. By contrast, relatively good agreement is achieved at large angular scales in the *WMAP*7 best-fitting cosmology, with all but the NOCOOL model being roughly consistent with the *Planck* power spectrum measurements. The lower power in the *WMAP*7 cosmology is due primarily to the lower values of σ_8 (0.81 versus 0.834) and Ω_{m} (0.272 versus 0.318).

Encouragingly, these results are qualitatively consistent with the findings of Planck Collaboration XXI (2013), who used a simple halo model analytical approach combined with the Tinker et al. (2008) mass function and the Arnaud et al. (2010) universal pressure profile to calculate a template tSZ power spectrum (see also Efstathiou & Migliaccio 2012). By adjusting the amplitude of the template tSZ power spectrum, Planck Collaboration XXI (2013)

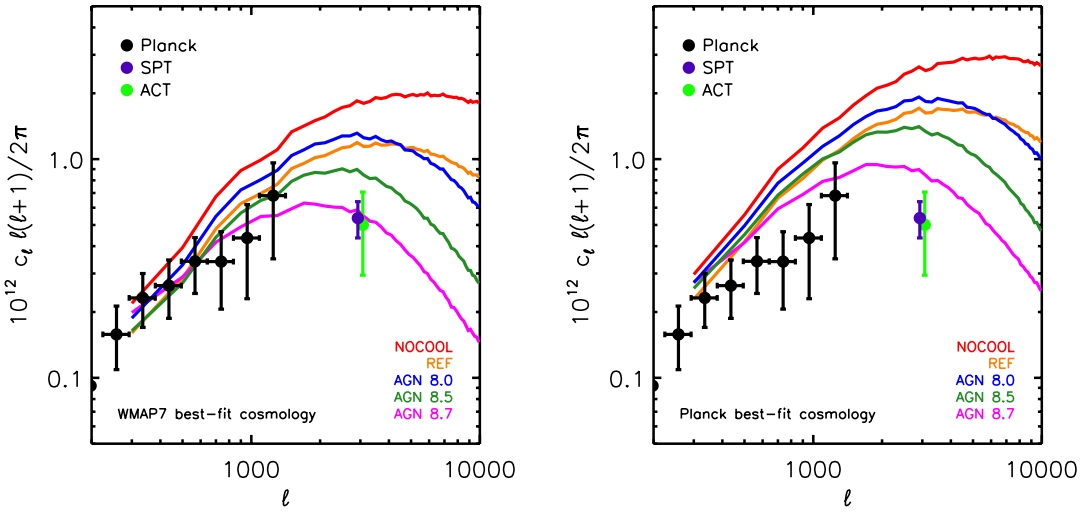

Figure 4. Comparison of observed and predicted tSZ angular power spectra in the *WMAP*7 best-fitting cosmology (left) and the *Planck* best-fitting cosmology (right). The thick coloured curves represent the mean power spectra for each of the simulations. The filled circles with 1σ error bars represent measurements from the *Planck* telescope (Planck Collaboration XXI 2013, black), the SPT (Reichardt et al. 2012, purple), and the ACT (Sievers et al. 2013, bright green), respectively. There is a significant amplitude offset between the models and the observations on all angular scales in the *Planck* cosmology. In the *WMAP*7 cosmology, by contrast, there is reasonable agreement at large angular scales. However, the fiducial AGN model (AGN 8.0), which reproduces the properties of local groups and clusters best, has a factor of $\sim$2 more power than observed by SPT and ACT at $\ell \approx 3000$.

derive the constraint $\sigma_8(\Omega_m/0.28)^{0.395} = 0.784 \pm 0.016$ (68 per cent C.L.), which is significantly lower than inferred from the *Planck* primary CMB, but is only 1σ lower than the *WMAP*7 best-fitting cosmology.

We point out that while there is qualitative agreement between our findings and those of the *Planck* team, some quantitative differences are present. Specifically, when we scale their best-fitting halo model to the cosmology adopted in our simulations, the amplitudes of the halo model and hydrodynamical simulation power spectra differ by up to 50 per cent at large angular scales, in the sense that the halo model predicts more power than the hydrodynamical simulations. As a consequence, the derived joint constraint on σ_8 and Ω_m using the halo model is roughly 1σ lower than what we would infer by scaling our simulations to match the observational data. Why the *Planck* halo model predicts more power than the hydrodynamical simulations at large scales (for a given cosmology) is unclear but is worth further investigation. We note that the simple halo model approach neglects the effects of asphericity and substructure, which Battaglia et al. (2012) have demonstrated to be relevant for the tSZ power spectrum. Furthermore, the analytic methodology neglects the relatively large intrinsic scatter in the tSZ flux of observed clusters (see e.g. fig. 8 of L14) and assumes self-similar evolution, although the addition of scatter and alternative assumptions about evolution should be straightforward to implement. Finally, recent simulation studies that include AGN feedback find that gas ejection can alter the halo mass function by up to $\sim$15–20 per cent at the massive end (e.g. Cusworth et al. 2014; Cui, Borgani & Murante 2014; Velliscig et al. 2014). By contrast, our hydrodynamical simulations implicitly include all of these effects, which may go some ways towards explaining differences with the halo model[3] predictions.

In spite of the relatively good agreement between the *WMAP*7 simulations and the observations on large scales and the ability of model AGN 8.0 to simultaneously reproduce many 'resolved' properties of the Local Group and cluster population remarkably well, the fiducial AGN model, AGN 8.0, is clearly inconsistent with the ACT and SPT measurements on intermediate angular scales ($\ell \approx 3000$). AGN models with higher heating temperatures perform much better in this regard, but cannot be reconciled with the properties of the Local Group and cluster population (see L14).

How can we interpret these findings? One possibility is that the redshift evolution of clusters in the fiducial AGN model is not quite correct, in the sense that real clusters could have lower densities and pressures than predicted by the model at high redshift (as shown in Fig. 3, the power spectrum at $\ell \sim 3000$ is sensitive to high-z clusters). However, observations appear to suggest that, if anything, the gas mass fractions increase with redshift (Lin et al. 2012). Direct comparison of the models with observations of high-redshift clusters will help clarify this question, but observational selection effects would have to be properly addressed.

Another possibility is that the contributions from Galactic dust emission, radio galaxies, and/or the cosmic infrared background (CIB) from stellar-heated dust within galaxies (which has both clustered and unclustered components) to the ACT and SPT total power spectra have for some reason been overestimated, resulting in an underestimate of the tSZ power spectrum amplitude.[4] Note that these experiments do not directly measure the tSZ power spectrum, but instead measure a total power spectrum from which the contributions of the primary CMB, radio sources, Galactic dust, the

[3] This is not to suggest that the halo model does not have its uses, quite the contrary; its strength lies in its ability to rapidly explore physical and cosmological parameter space, as well as probing the largest angular scales not easily accessible with self-consistent hydrodynamical simulations (e.g. Hill & Pajer 2013).

[4] This potential caveat is also applicable to the *Planck* tSZ power spectrum measurements. The dominant foreground for *Planck* is thought to be the CIB and the analysis of the *Planck* data adopts a prior $A_{CIB} = 1 \pm 0.5$ on the amplitude of this component. If in reality the CIB contributes negligibly to the total power, however, then this would result in a $\sim$30 per cent boost to the inferred *Planck* tSZ power spectrum measurements (Seljak, private communication).

CIB, and kSZ are removed by adjusting template models for each component.

Alternatively, the *WMAP*7 best-fitting cosmology may not be quite correct. The agreement on large scales may suggest that it is not far from the truth, but the amplitude, and to some extent the shape, of the tSZ power spectrum is very sensitive to the adopted cosmological parameters. This, of course, is one of the primary reasons why measurements of the tSZ power spectrum are being made. It is therefore of interest to see what the implications are of the uncertainty in the cosmological parameters for the above comparisons. Below we employ the primary CMB Markov chain Monte Carlo (MCMC) runs carried out by the *WMAP*7 and *Planck* teams to explore the impact of the uncertainty on the cosmological parameters inferred by *WMAP*7 and *Planck* on the predicted tSZ angular power spectrum.

5.1 Impact of uncertainty in cosmological parameters

To ascertain the impact of uncertainty in the values of the cosmological parameters on the predicted tSZ power spectrum, we need a method to scale the simulated power spectra to arbitrary cosmologies (unfortunately the simulations are too expensive to run a large grid of cosmologies). The tSZ power spectrum is most sensitive to the matter power spectrum normalization, σ_8, but there are also relevant dependencies on the other parameters of the Λ cold dark matter (ΛCDM) model. To complicate things further, the relative contributions change as a function of angular scale.

Millea et al. (2012) have used the semi-analytic cluster model of Shaw et al. (2010) (which is an extension of the models originally developed by Ostriker, Bode & Babul 2005; Bode, Ostriker & Vikhlinin 2009) to construct a data base of tSZ power spectra for a large grid of cosmologies. The Shaw et al. model has simplified treatments of feedback due to AGN and supernovae (calibrated to reproduce the gas and stellar mass fractions of local clusters), as well as a prescription for radially varying non-thermal pressure support[5] calibrated using numerical simulations (Nagai et al. 2007). Millea et al. (2012) fit for the dependencies of the power spectrum amplitude, as a function of multipole, of five cosmological parameters: $\Omega_{\rm m}$, $\Omega_{\rm b}$, σ_8, $n_{\rm s}$, and h (Ω_Λ is fixed by the assumption of a flat universe). Although the derived dependencies are expected to be somewhat model dependent, they should represent an improvement over the simple σ_8^n (where n is constant $\approx$8) scaling applied in many previous studies.

In Fig. 5 we test the validity of the scalings proposed by Millea et al. (2012) for our hydrodynamical simulations, by comparing how well the power spectra from our *WMAP*7 best-fitting cosmology runs agree with those from our *Planck* best-fitting cosmology runs when the former are scaled to the *Planck* cosmology.

As is visible from the bottom panel of Fig. 5, the scalings are generally accurate to $\approx$10–15 per cent. They perform slightly better than average at $\ell \sim 3000$ ($\approx$5–10 per cent accuracy), which is where the discrepancy between the simulations and observations is largest. Bearing this accuracy in mind, we now proceed to use the scalings of Millea et al. (2012) to quantify the uncertainty in the predicted tSZ power spectrum due to uncertainties in cosmological parameters constrained by primary CMB measurements.

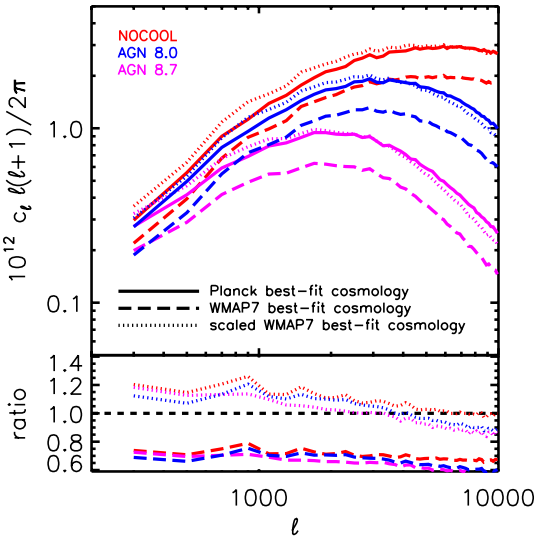

Figure 5. Testing the cosmological parameter scalings proposed by Millea et al. (2012) for the tSZ power spectrum. Top: the solid and dashed curves represent simulations carried out with the *Planck* and *WMAP*7 best-fitting cosmologies, respectively. The dotted curves represent the *WMAP*7 runs scaled to the *Planck* cosmology using the scalings of Millea et al. (2012). Bottom: the dashed curves represent the ratio of the *WMAP*7 to *Planck* cosmology runs, while the dotted curves represent the ratio of the scaled *WMAP*7 results to the *Planck* cosmology runs. The scalings are accurate to $\approx$5–10 per cent at $\ell \sim 3000$ and generally accurate to $\approx$10–15 per cent.

We sample the MCMC data[6] produced by the *WMAP*7 and *Planck* teams, randomly selecting 1000 sets of cosmological parameter values from each. For a given set of parameter values we use the scalings proposed by Millea et al. (2012) to adjust the tSZ power spectrum predicted by the fiducial AGN model. We thus construct 1000 power spectra for the model for both the *WMAP*7 and *Planck* cases. In Fig. 6 we plot the range of power spectra that is allowed (2σ confidence region) by the *WMAP*7 and *Planck* primary CMB data, i.e. we have propagated the uncertainties in the primary CMB cosmological parameters to an uncertainty in the predicted tSZ angular power spectrum.

In terms of the *Planck* primary CMB constraints, the predicted tSZ power spectrum is consistent with individual *Planck* power spectrum measurements ($\ell \lesssim 1000$) at the $\approx 2\sigma$ level (each). How large the discrepancy is with the data set as a whole depends on the degree of covariance between neighbouring C_ℓs for both the observational data and the theoretical predictions. We note that the *Planck* team have binned their data so as to minimize the covariance between neighbouring points at large scales and to maximize the signal-to-noise ratio at small scales. Without reproducing their analysis methods exactly, it is difficult to precisely deduce the level of the discrepancy with the data set but a (likely overly) conservative lower limit is 2σ. Given the *Planck* primary CMB constraints, the predicted power spectra are obviously highly inconsistent with the ACT and SPT measurements at $\ell \approx 3000$.

The constraints placed by the *WMAP*7 primary CMB analysis, on the other hand, are fully consistent with the *Planck* power spectrum measurements and also consistent with the ACT and SPT measurements at the 2σ level (see shaded region). We note, however, that no single set of parameter values (i.e. no individual chain) yields a

[5] Our cosmological hydrodynamical simulations implicitly include non-thermal pressure support due to non-virialized gas.

[6] Publicly available on the *WMAP*7 and *Planck* websites.

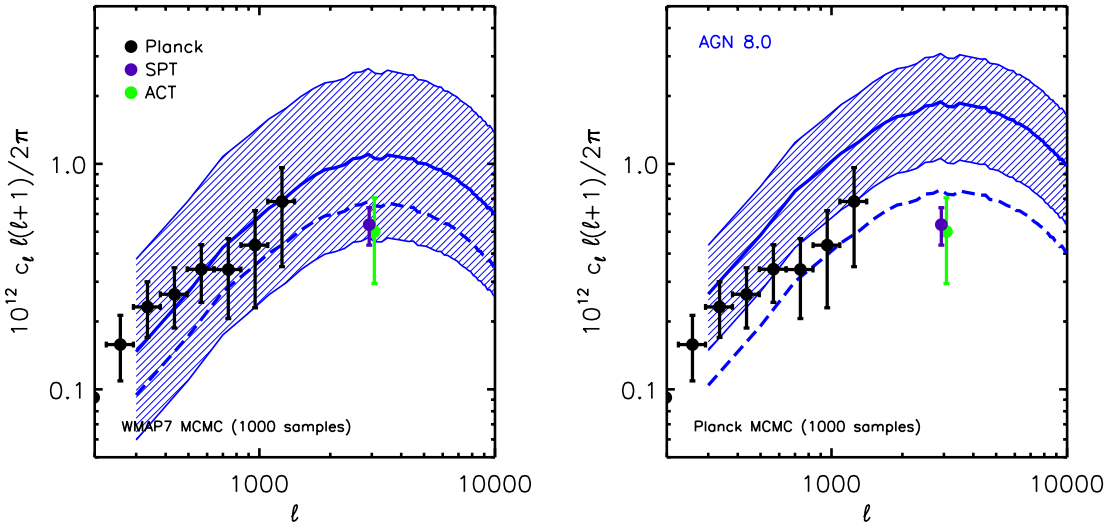

Figure 6. Impact of primary CMB cosmological parameter uncertainties on the predicted tSZ angular power spectrum, using the fiducial AGN model (AGN 8.0). Left: using the *WMAP*7 MCMCs. Right: using the *Planck* MCMCs. The shaded region represents the uncertainty in the predicted tSZ power spectrum given the range of cosmologies allowed by the *WMAP*7 and *Planck* primary CMB constraints. The shaded region encloses 95 per cent (2σ) of the distribution (power spectrum at a given multipole) and the thick solid curve represents the median relation. The thick dashed curve represents the chain that gives the best match to the observed C_ℓ data. The filled circles with 1σ error bars represent measurements from the *Planck* telescope (black), the SPT (purple), and the ACT (bright green), respectively. The predictions of the fiducial AGN model, AGN 8.0, are highly inconsistent with the *Planck* and the SPT and ACT measurements using the range of ΛCDM models allowed by the *Planck* primary CMB analysis. They are, however, fully consistent with the *Planck* power spectrum measurements and are consistent with the SPT and ACT data at the $\sim 2\sigma$ level using the range of cosmological models allowed by the *WMAP*7 primary CMB analysis.

formally good fit to the *Planck*, SPT, and ACT data[7] simultaneously in the context of the fiducial AGN model (see dashed curve in the left-hand panel of Fig. 6). The best-fitting set of parameter values, obtained for the case $\sigma_8 \approx 0.766$ and $\Omega_m \approx 0.280$, has a reduced $\chi^2 \approx 2.2$. Adopting the AGN 8.5 model does result in a formally acceptable fit (with a reduced $\chi^2 \approx 1.2$ for $\sigma_8 \approx 0.777$ and $\Omega_m \approx 0.289$) but, as already discussed, this model is in some tension with the observed properties of local groups and clusters.

In summary, if we adopt the range of ΛCDM models allowed by the *WMAP*7 primary CMB data, we conclude that it is possible to construct a model that is consistent with the tSZ power spectrum measurements on large scales, and within 2σ of the data on intermediate scales, as well as with the known 'resolved' properties of local groups and clusters. By contrast, the predicted tSZ power spectra are inconsistent with the power spectrum measurements on large and intermediate scales when the range of ΛCDM models allowed is constrained by the *Planck* primary CMB data. To reconcile the *Planck* primary CMB constraints with the observed power spectrum measurements requires there to be either a very different evolution in the cluster population in the models compared to reality,[8] a departure from standard ΛCDM, or else that the tSZ power spectrum measurements are significantly biased low, e.g. due to an overestimate of the contribution of Galactic dust, radio galaxies, or the CIB to the total power spectrum.

[7] We have neglected the covariance between the *Planck* data points for this comparison.

[8] We have experimented with adjusting the amplitude of the deconstructed power spectra in bins of redshift for the fiducial AGN model in the *Planck* best-fitting cosmology. To match the *Planck* measurements at large angular scales requires a factor of ≈3 suppression at redshifts $z \gtrsim 0.25$, while to match the SPT/ACT measurements requires another factor of ≈2 suppression for sources with $z \gtrsim 0.5$ (so a total of ≈6). Assuming the gas remains at approximately the virial temperature, this implies gas mass reductions of $\approx\sqrt{3}$ and $\approx\sqrt{6}$, respectively, for haloes with masses of $\gtrsim 10^{14}\ M_\odot$. The former requirement appears to conflict with direct observational measurements (Lin et al. 2012).

6 COMPARISON TO PREVIOUS STUDIES

Many previous theoretical studies have examined the tSZ power spectrum (e.g. da Silva et al. 2001; Springel, White & Hernquist 2001; Komatsu & Seljak 2002; White et al. 2002; Roncarelli et al. 2006; Holder et al. 2007; Battaglia et al. 2010, 2012; Sehgal et al. 2010; Shaw et al. 2010). Generally speaking, models developed prior to the first measurements of the tSZ power spectrum (by the SPT) predicted powers significantly higher than were later observed, even when the adopted cosmology was consistent with *WMAP* constraints. This is likely a result of many of these early models neglecting efficient feedback from AGN, which is necessary to reconcile the models with the observed low gas densities of groups and clusters (e.g. Bower et al. 2008; Puchwein et al. 2008; McCarthy et al. 2010). As we have shown above (Fig. 4), such gas ejection can strongly reduce the amplitude of the predicted tSZ power spectrum on intermediate angular scales.

Two of the more recent studies which have included energy input from a central engine are Shaw et al. (2010) and Battaglia et al. (2010, 2012), with both predicting a tSZ power spectrum in approximate consistency with the SPT and ACT measurements for their adopted cosmologies. It is therefore of interest to see how our results compare with these previous studies and to see, in particular, how robust our conclusions are on the discrepancy with the *Planck* best-fitting cosmology that we reported above.

In the left-hand panel of Fig. 7 we compare our predicted tSZ power spectra with the non-radiative and AGN feedback models of Battaglia et al. (2012). Encouragingly, there is excellent consistency between the non-radiative simulations of these authors and our own NOCOOL model. Interestingly, their AGN model predicts

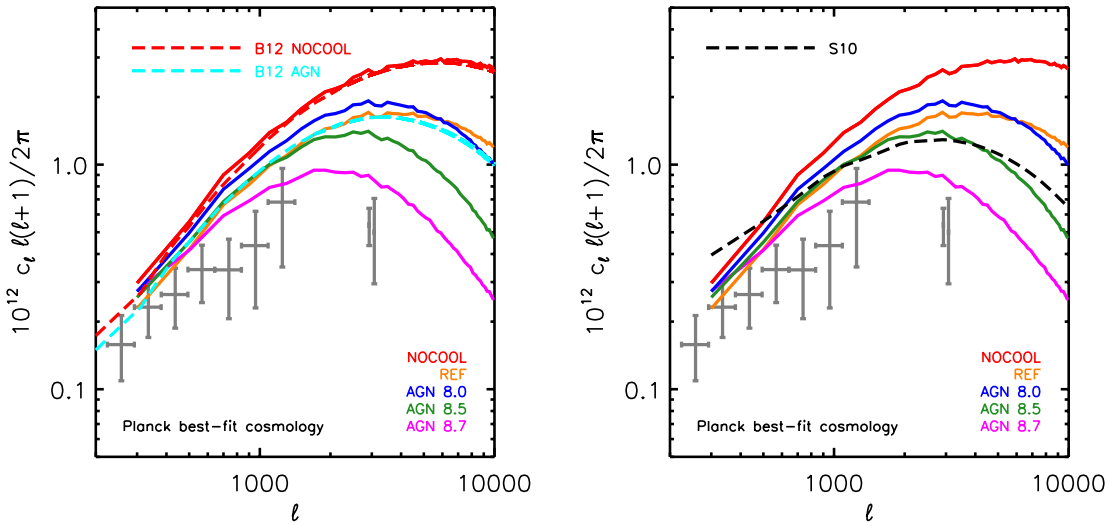

Figure 7. Comparison with the tSZ power spectra from (left) the SPH simulations of Battaglia et al. (2012) (B12) and (right) from the analytical model of Shaw et al. (2010) (S10). We have scaled the power spectra of Battaglia et al. (2012) and Shaw et al. (2010) to the *Planck* best-fitting cosmology using the formalism of Millea et al. (2012). The grey data points with 1σ errors bars represent the measurements from the *Planck* telescope, SPT, and ACT, as in previous figures. All of the models are highly inconsistent with the ACT and SPT power spectrum measurements if the *Planck* best-fitting cosmology is assumed. Note the excellent consistency of the B12 and all of our simulations at large angular scales.

a tSZ power spectrum that is similar to our fiducial AGN model. This is understandable at large angular scales (where all the simulations converge), but the agreement at intermediate and small angular scales is a bit surprising at first sight, given the sensitivity of these scales to non-gravitational physics. It is surprising because there are large differences in the subgrid implementations of radiative cooling (they assume primordial cooling only, whereas our simulations include metal-line cooling computed on an element-by-element basis) and AGN feedback (their feedback scales with the integrated star formation rate of their haloes, whereas ours scales with the local Bondi accretion rate), both of which can change the *qualitative* properties of groups and clusters (McCarthy et al. 2011). The similarity may be tied to the fact that the AGN model of Battaglia et al. (2012) was tuned to match the gas and stellar mass fractions of a higher resolution zoomed simulation run with the more detailed AGN model of Sijacki et al. (2008), which, similar to our fiducial model, reproduces the baryon fractions of local groups and clusters reasonably well.

The consistency between all the simulations at large angular scales, independent of subgrid physics, bodes well for the use of this region of the power spectrum for cosmological purposes. It also indicates that the box sizes of current cosmological hydrodynamical simulations are sufficiently large to capture the power on these angular scales (note that the B12 simulations have box sizes of $165\,h^{-1}$ Mpc, compared to the $400\,h^{-1}$ Mpc boxes used here).

In the right-hand panel of Fig. 7 we compare to the semi-analytic model of Shaw et al. (2010). The Shaw et al. (2010) model combines a simple model for the re-distribution of the hot gas due to star formation, feedback from AGN, and radially varying non-thermal pressure support. The star formation efficiency and feedback parameters are tuned to match some of the properties of the Local Group and cluster population, while the non-thermal pressure support is constrained using cosmological simulations. This cluster physics prescription is combined with the mass function of Tinker et al. (2008) to make predictions for the tSZ power spectrum. Their model predicts a power spectrum that is similar to our AGN 8.5 model at intermediate and small angular scales. There is puzzling offset from the simulation-based power spectra at large angular scales, whose origin is unclear. These scales probe large physical radii (beyond the virial radius), suggesting the difference may be due to departures from spherical symmetry and/or an increasing importance of substructure, which are absent in the halo model approach. Alternatively, it may signal an issue in their parametrization of the contribution of non-thermal pressure support, which becomes increasingly important at large radii.

Overall, from Fig. 7 we conclude that *none* of the current tSZ power spectrum predictions is consistent with the *Planck* and (particularly) the SPT and ACT measurements if the *Planck* best-fitting cosmology is adopted.

7 SUMMARY AND DISCUSSION

We have employed the cosmo-OWLS suite of large-volume cosmological hydrodynamical simulations (described in detail in Le Brun et al. 2014) to explore the astrophysical and cosmological dependencies of the tSZ power spectrum. cosmo-OWLS is an extension of the OWLS project (Schaye et al. 2010) and has been designed specifically to aid the interpretation and analysis of cluster cosmology and large-scale structure surveys.

From the analysis presented here, we arrive at several important conclusions.

(i) For a given cosmology, the tSZ signal on intermediate and small scales ($\ell \gtrsim 1000$) is highly sensitive to important subgrid physics (Fig. 4), owing to the fact this range of scales probes intermediate radii in clusters (Fig. 3) which are susceptible to non-gravitational processes such as gas ejection due to AGN feedback (e.g. McCarthy et al. 2011). However, at larger scales ($\ell \ll 1000$), which probe gas at large physical radii around nearby relatively massive clusters, the effects of 'subgrid' physics are minor.

(ii) For a given physical model, the tSZ signal on all accessible scales is very sensitive to cosmological parameters that affect the abundance of the clusters, particularly σ_8 and $\Omega_{\rm m}$. Given the insensitivity of the signal to non-gravitational physics at large angular

scales, this likely represents the best regime for deriving cosmological constraints.

(iii) *We find a significant amplitude offset between all the simulations and the observations of the tSZ power spectrum on all measured angular scales, if the Planck best-fitting cosmology is assumed by the simulations, with the simulations predicting more power than is observed* (Figs 4 and 6, right-hand panel). This includes the large angular scales probed by the *Planck* satellite, which are insensitive to assumptions about subgrid physics. Note also that one of the models, the fiducial AGN model (AGN 8.0), reproduces the global X-ray, tSZ, optical, and BH scaling relations (see Le Brun et al. 2014), as well as the observed pressure distribution of the hot gas (Fig. 2) of the Local Group and cluster population.

(iv) By contrast, if the *WMAP*7 cosmology is adopted by the simulations, there is full consistency with the *Planck* power spectrum measurements on large scales and agreement at the 2σ level for SPT and ACT measurements of the power spectrum at intermediate scales for the fiducial AGN model (Figs 4 and 6, left-hand panel). We note, however, that no single set of cosmological parameter values (in a standard six-parameter ΛCDM model) yields a formally acceptable fit to the *Planck*, SPT, and ACT data simultaneously using our fiducial AGN model.

(v) In the *WMAP*7 cosmology it is possible to match the SPT and ACT measurements by making the AGN feedback more violent and bursty than in the fiducial AGN model (Fig. 4, left-hand panel), but this comes at the expense of spoiling the excellent agreement with the 'resolved' properties of local clusters (Le Brun et al. 2014).

(vi) To reconcile the *Planck* primary CMB constraints with the observed power spectrum (particularly the ACT and SPT measurements), there would have to be either a very different evolution in the cluster population in the models compared to reality (such that real clusters must be significantly underdense/underpressurized compared to the models at high-z, but observations suggest otherwise; Lin et al. 2012), a departure from standard ΛCDM, or else that the tSZ power spectrum data are significantly biased low, e.g. due to an overestimate of the contribution of Galactic dust, radio galaxies, or the cosmic infrared background to the total power spectrum.

(vii) By comparing our results with previous theoretical studies (namely Shaw et al. 2010; Battaglia et al. 2012), we show that the above conclusions are generic to current models.

The simplest interpretation of our findings is that the lower-than-expected amplitude of the tSZ power spectrum indicates that there are significantly fewer massive dark matter haloes than expected for the *Planck* primary CMB cosmology. Indeed, Planck Collaboration XXI (2013) placed constraints on σ_8 and Ω_m using a simple halo-model-based approach to the tSZ power spectrum and concluded there was tension with the values derived from the primary CMB. Interestingly, they noted that the derived constraints were fully consistent with those obtained from the tSZ cluster number counts in Planck Collaboration XX (2013). In spite of this consistency, Planck Collaboration XXI (2013) suggest that the discrepancy with the primary CMB constraints is likely tied to systematics in the cluster modelling which affects both the number counts and power spectrum analyses, but in different ways. For example, if the hydrostatic mass bias is significantly larger than currently thought, this would have the effect of lowering the number of haloes above a given tSZ flux. At the same time, this mass bias would introduce an error in the halo modelling approach of the power spectrum, since it adopts empirical constraints between the tSZ flux signal and halo mass (namely the universal pressure profile of Arnaud et al. 2010).

However, we have shown here that a significant discrepancy exists in the amplitude of the predicted and observed tSZ power spectrum that does not rely on the tSZ flux–mass relation being known, and also addresses other criticisms of the halo model approach (e.g. asphericity, substructure, intrinsic scatter, a halo mass function that includes modifications due to baryons). We simply compare the power spectra of simulated and observed tSZ skies, where the simulated tSZ skies are produced from fully self-consistent cosmological hydrodynamical simulations including one that reproduces optical and X-ray observations of local groups and clusters. We point out that our results are consistent with other *Planck* tSZ-derived constraints on σ_8 and Ω_m, including those derived from the cross-correlation of X-ray clusters (Hajian et al. 2013) and CMB lensing (Hill & Spergel 2013) with the *Planck* tSZ signal, as well as constraints from galaxy–galaxy lensing and galaxy clustering (e.g. Cacciato et al. 2013).

At face value, therefore, our results pose a significant challenge to the cosmological parameter values preferred (and/or the model adopted) by the *Planck* primary CMB analyses. To be definitive, however, confirmation of these findings using other simulations is needed. Furthermore, a more rigorous comparison between the simulated tSZ skies and observations should be undertaken, by bringing the simulated tSZ skies fully to the observational plane (instrumental response+noise+contamination) and then analysing them using the same pipeline as used on the real data. In addition, since the power spectrum is sensitive to high-z clusters, it will be important to confront the models with resolved observations of such systems (but care must be taken to address important observational selection effects).

While finalizing this paper a re-analysis of the *Planck* primary CMB data by Spergel et al. (2013) was posted to the arXiv. These authors claim to have identified a systematic issue with the 217×217 GHz^2 detector set spectrum used in the *Planck* analysis. When corrected for, Spergel et al. (2013) find that some of the tension between the *Planck* best-fitting parameters and previous cosmological constraints is removed. We have used the best-fitting cosmological parameters derived by Spergel et al. (2013) to see what impact this has on the predicted tSZ power spectrum. We scale the simulated power spectra to the Spergel et al. best-fitting cosmology. The results are shown in Fig. 8 and show that the amplitude offset is significantly reduced for this revised cosmology.

ACKNOWLEDGEMENTS

The authors would like to thank the referee, Stefano Borgani, for useful suggestions which improved the quality of the paper. They also thank the members of the OWLS team for their contributions to the development of the simulation code used here, as well as Nick Battaglia, George Efstathiou, Colin Hill, Scott Kay, Eiichiro Komatsu, Uros Seljak, David Spergel, and Simon White for helpful discussions. Further thanks to Nick Battaglia for providing his simulated power spectra and Ming Sun for providing his pressure profile measurements. IGM is supported by an STFC Advanced Fellowship at Liverpool John Moores University. AMCLB acknowledges support from an internally funded PhD studentship at the Astrophysics Research Institute of Liverpool John Moores University. JS is sponsored by the European Research Council under the European Union's Seventh Framework Programme (FP7/2007-2013)/ERC Grant agreement 278594-GasAroundGalaxies. This work used the DiRAC Data Centric system at Durham University, operated by the Institute for Computational Cosmology on behalf of the STFC DiRAC HPC Facility (www.dirac.ac.uk). This

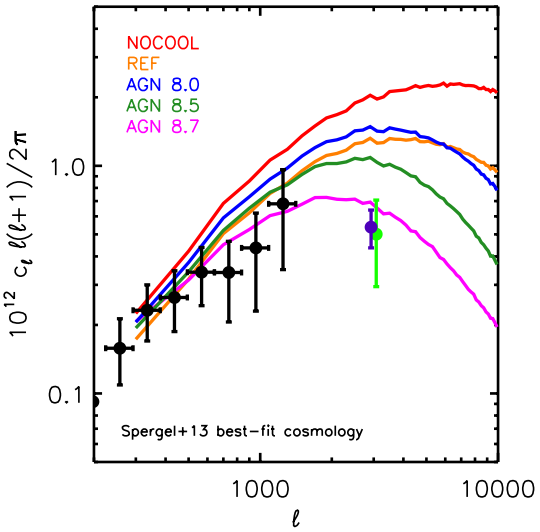

Figure 8. The tSZ power spectra in a Spergel, Flauger & Hlozek (2013) best-fitting cosmology. The amplitude offset with respect to the data is now largely removed and predicted spectra are very similar to that obtained in *WMAP7* best-fitting cosmology (see left-hand panel of Fig. 4).

equipment was funded by BIS National E-infrastructure capital grant ST/K00042X/1, STFC capital grant ST/H008519/1, and STFC DiRAC Operations grant ST/K003267/1 and Durham University. DiRAC is part of the National E-Infrastructure.

REFERENCES

Arnaud M., Pratt G. W., Piffaretti R., Böhringer H., Croston J. H., Pointecouteau E., 2010, A&A, 517, A92
Battaglia N., Bond J. R., Pfrommer C., Sievers J. L., Sijacki D., 2010, ApJ, 725, 91
Battaglia N., Bond J. R., Pfrommer C., Sievers J. L., 2012, ApJ, 758, 75
Birkinshaw M., 1999, Phys. Rep., 310, 97
Bode P., Ostriker J. P., Vikhlinin A., 2009, ApJ, 700, 989
Böhringer H. et al., 2007, A&A, 469, 363
Booth C. M., Schaye J., 2009, MNRAS, 398, 53
Bower R. G., McCarthy I. G., Benson A. J., 2008, MNRAS, 390, 1399
Cacciato M., van den Bosch F. C., More S., Mo H., Yang X., 2013, MNRAS, 430, 767
Carlstrom J. E., Holder G. P., Reese E. D., 2002, ARA&A, 40, 643
Cui W., Borgani S., Murante G., 2014, MNRAS, preprint (arXiv:1402.1493)
Cusworth S. J., Kay S. T., Battye R. A., Thomas P. A., 2014, MNRAS, 439, 2485
Dalla Vecchia C., Schaye J., 2008, MNRAS, 387, 1431
da Silva A. C., Barbosa D., Liddle A. R., Thomas P. A., 2000, MNRAS, 317, 37
da Silva A. C., Kay S. T., Liddle A. R., Thomas P. A., Pearce F. R., Barbosa D., 2001, ApJ, 561, L15
Efstathiou G., Migliaccio M., 2012, MNRAS, 423, 2492
Hajian A., Battaglia N., Spergel D. N., Bond J. R., Pfrommer C., Sievers J. L., 2013, J. Cosmol. Astropart. Phys., 11, 64
Hand N. et al., 2012, Phys. Rev. Lett., 109, 041101
Hill J. C., Pajer E., 2013, Phys. Rev. D, 88, 063526
Hill J. C., Spergel D. N., 2013, J. Cosmol. Astropart. Phys., preprint (arXiv:1312.4525)
Holder G. P., McCarthy I. G., Babul A., 2007, MNRAS, 382, 1697
Jenkins A., Frenk C. S., White S. D. M., Colberg J. M., Cole S., Evrard A. E., Couchman H. M. P., Yoshida N., 2001, MNRAS, 321, 372
Komatsu E., Kitayama T., 1999, ApJ, 526, L1
Komatsu E., Seljak U., 2002, MNRAS, 336, 1256
Komatsu E. et al., 2011, ApJS, 192, 18
Le Brun A. M. C., McCarthy I. G., Schaye J., Ponman T. J., 2014, MNRAS, preprint (arXiv:1312.5462)
Lin Y.-T., Stanford S. A., Eisenhardt P. R. M., Vikhlinin A., Maughan B. J., Kravtsov A., 2012, ApJ, 745, L3
McCarthy I. G. et al., 2010, MNRAS, 406, 822
McCarthy I. G., Schaye J., Bower R. G., Ponman T. J., Booth C. M., Dalla Vecchia C., Springel V., 2011, MNRAS, 412, 1965
Millea M., Doré O., Dudley J., Holder G., Knox L., Shaw L., Song Y.-S., Zahn O., 2012, ApJ, 746, 4
Mo H., van den Bosch F. C., White S., 2010, Galaxy Formation and Evolution. Cambridge Univ. Press, Cambridge
Nagai D., Kravtsov A. V., Vikhlinin A., 2007, ApJ, 668, 1
Ostriker J. P., Bode P., Babul A., 2005, ApJ, 634, 964
Planck Collaboration XVI, 2013, A&A, preprint (arXiv:1303.5076)
Planck Collaboration XX, 2013, A&A, preprint (arXiv:1303.5080)
Planck Collaboration XXI, 2013, A&A, preprint (arXiv:1303.5081)
Planelles S., Borgani S., Fabjan D., Killedar M., Murante G., Granato G. L., Ragone-Figueroa C., Dolag K., 2014, MNRAS, 438, 195
Puchwein E., Sijacki D., Springel V., 2008, ApJ, 687, L53
Reichardt C. L. et al., 2012, ApJ, 755, 70
Roncarelli M., Moscardini L., Tozzi P., Borgani S., Cheng L. M., Diaferio A., Dolag K., Murante G., 2006, MNRAS, 368, 74
Roncarelli M., Moscardini L., Borgani S., Dolag K., 2007, MNRAS, 378, 1259
Sayers J. et al., 2013, ApJ, 778, 52
Schaye J., Dalla Vecchia C., 2008, MNRAS, 383, 1210
Schaye J. et al., 2010, MNRAS, 402, 1536
Sehgal N., Bode P., Das S., Hernandez-Monteagudo C., Huffenberger K., Lin Y.-T., Ostriker J. P., Trac H., 2010, ApJ, 709, 920
Shaw L. D., Nagai D., Bhattacharya S., Lau E. T., 2010, ApJ, 725, 1452
Short C. J., Thomas P. A., 2009, ApJ, 704, 915
Sievers J. L. et al., 2013, J. Cosmol. Astropart. Phys., 10, 60
Sijacki D., Pfrommer C., Springel V., Enßlin T. A., 2008, MNRAS, 387, 1403
Spergel D., Flauger R., Hlozek R., 2013, preprint (arXiv:1312.3313)
Springel V., 2005, MNRAS, 364, 1105
Springel V., White M., Hernquist L., 2001, ApJ, 549, 681
Springel V., Di Matteo T., Hernquist L., 2005, MNRAS, 361, 776
Sun M., Sehgal N., Voit G. M., Donahue M., Jones C., Forman W., Vikhlinin A., Sarazin C., 2011, ApJ, 727, L49
Sunyaev R. A., Zeldovich Y. B., 1972, Comments Astrophys. Space Phys., 4, 173
Tinker J., Kravtsov A. V., Klypin A., Abazajian K., Warren M., Yepes G., Gottlöber S., Holz D. E., 2008, ApJ, 688, 709
Trac H., Bode P., Ostriker J. P., 2011, ApJ, 727, 94
van Daalen M. P., Schaye J., McCarthy I. G., Booth C. M., Dalla Vecchia C., 2013, MNRAS, preprint (arXiv:1310.7571)
Velliscig M., van Daalen M. P., Schaye J., McCarthy I. G., Cacciato M., Le Brun A. M. C., Dalla Vecchia C., 2014, MNRAS, preprint (arXiv:1402.4461)
Voit G. M., 2005, Rev. Modern Phys., 77, 207
White M., Hernquist L., Springel V., 2002, ApJ, 579, 16
Wiersma R. P. C., Schaye J., Smith B. D., 2009a, MNRAS, 393, 99
Wiersma R. P. C., Schaye J., Theuns T., Dalla Vecchia C., Tornatore L., 2009b, MNRAS, 399, 574

APPENDIX A: RESOLUTION STUDY

In Fig. A1 we present a numerical resolution convergence study for the predicted tSZ power spectra. For this test we use 100 h^{-1} Mpc box simulations with 256^3 (fiducial) and 512^3 (high resolution) baryon and dark matter particles. The latter has a factor of 8 (2) better mass (spatial) resolution than the former. (Note that a 400 h^{-1} Mpc box with 1024^3 particles has the same resolution as a 100 h^{-1} Mpc box with 256^3 particles.) The smaller box size imposes a smaller

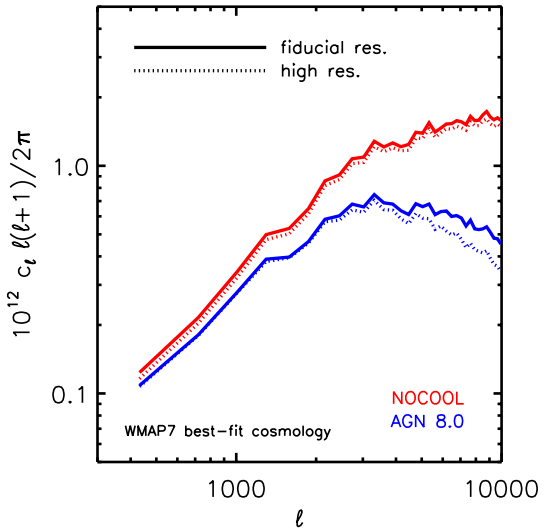

Figure A1. Predicted tSZ power spectra for the fiducial and high-resolution simulations. These are based on $1\overset{\circ}{.}25 \times 1\overset{\circ}{.}25$ surveys constructed from $100\,h^{-1}$ Mpc simulations with 256^3 (fiducial) and 512^3 (high resolution) baryon and dark matter particles. The tSZ power spectra are reasonably well converged at all angular scales in the NOCOOL run and at $\ell \lesssim 4000$ for the fiducial AGN run.

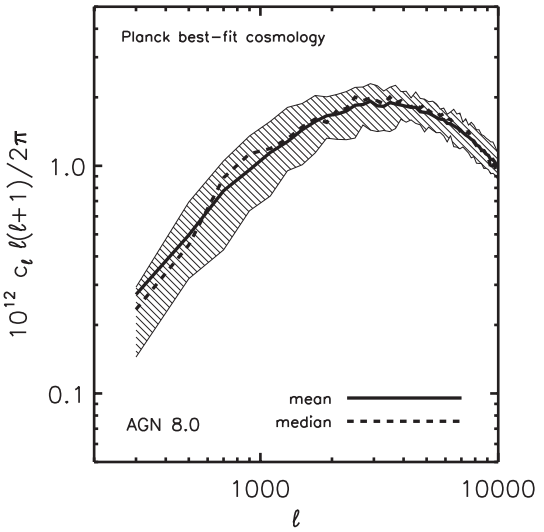

Figure B1. Map-to-map scatter in the predicted tSZ power spectrum for the fiducial AGN model for the 25 deg^2 maps. The solid and dashed curves represent the mean and median power spectra from the 10 light cone realizations. The shaded region encloses the 10th and 90th percentiles. At large angular scales ($\ell \lesssim 1000$) the scatter in the power spectrum can reach ∼50 per cent, while at small scales ($\ell \gtrsim 3000$) it is typically ∼20 per cent.

field of view, we thus construct $1\overset{\circ}{.}25 \times 1\overset{\circ}{.}25$ light cones back to $z = 3$.

The tSZ power spectra are well converged at all angular scales in the NOCOOL run and at $\ell \lesssim 4000$ for the fiducial AGN run. At $\ell = 10000$ the high-resolution simulation has ≈25 per cent less power compared to the fiducial run.

APPENDIX B: COSMIC VARIANCE

In Fig. B1 we show the map-to-map scatter in the predicted tSZ power spectra for the fiducial AGN model in the *Planck* best-fitting cosmology. The shaded region encloses the 10th and 90th percentiles. The scatter can reach up to ∼50 per cent at large angular scales ($\ell \lesssim 1000$), but is typically only ∼20 per cent at intermediate/small scales ($\ell \gtrsim 3000$).

We stress that such cosmic variance is likely negligible for current large observational surveys which have areas of hundreds and thousands of square degrees. It is also negligible for simple halo model calculations which can probe arbitrarily large volumes. For self-consistent cosmological hydrodynamical simulations, such as the ones presented in this paper, it is crucial that the volume is sufficiently large (and/or the number of independent volumes analysed is sufficiently large) to be able to robustly estimate the true mean tSZ power spectrum on the range of scales of interest. The fact that there is excellent agreement between our mean power spectra at large angular scales, which were extracted from the same simulation and are thus not independent, and that of the simulations of Battaglia et al. (2012) (see the left-hand panel of Fig. 7), who use 10 independent but smaller volumes, indicates that current hydrodynamical simulations are sufficiently large to measure the mean power spectrum accurately.

This paper has been typeset from a TEX/LATEX file prepared by the author.